Relaxation processes of the infrared-active lattice phonons of crystalline CO_2

Roberto Bini,* Hans Jörg Jodl,† and Salvatore Califano
European Laboratory for Non-Linear Spectroscopy, Largo E. Fermi 2, 50125 Firenze, Italy
(Received 17 October 1991)

The bandwidths of the two infrared-active lattice phonons T_u^- at 68 cm^{-1} and T_u^+ at 117 cm^{-1} of crystalline CO_2 have been measured by Fourier-transform infrared spectroscopy as a function of temperature in the range 12–100 K. Single crystals of different thickness, from 25 to 100 μm, were grown in a low-temperature cell. The techniques for growing single crystals of suitable thickness and for handling the experimental data are presented in detail. The correction of the interferograms for the presence of interference fringes, due to multiple reflections on the cell windows, and the determination of the baseline are discussed. It is shown that Lorentzian functions fit the band profiles perfectly throughout the examined temperature range. The evolution with temperature of both bandwidths is clearly nonlinear and parallels that of the three Raman-active lattice phonons. As predicted by lattice-dynamical calculations, the width of the low-frequency T_u^- phonon is more than one order of magnitude smaller than that of the higher-frequency T_u^+ phonon. The interpretation of the experimental data is made in terms of elementary relaxation processes involving third- and fourth-order phonon-phonon coupling mechanisms. For completeness the interpretation is extended also to the Raman-active phonons. Calculations made at the lowest order (λ^2), using the whole two-phonon density of states and a single average phonon-phonon coupling coefficient, show that the largest contribution to the bandwidth arises in all cases from three-phonon decay processes. At the higher order (λ^4) it is shown that the dominant process, responsible for the nonlinear temperature dependence, can be well described by a diagram with four cubic coupling terms. The contribution of this diagram is proportional to the square of a phonon occupation number. The temperature dependence of the frequency of the five optical lattice phonons is also presented.

INTRODUCTION

Experimental and theoretical research on phonon relaxation processes in molecular crystals has been rapidly growing in the past few years, owing to the very specific information they furnish on the dynamics of these crystals, in particular on dynamical processes controlled by the anharmonicity of the intermolecular potential. Experimental data are essentially collected in the frequency domain by bandwidth measurements using high-resolution Raman spectroscopy[1] or in the time domain by time-resolved coherent anti-Stokes Raman spectroscopy (CARS).[2] The theoretical interpretation of these results is basically made by identification of suitable decay or dephasing mechanisms, governed by anharmonic phonon-phonon interactions. These are conveniently handled in terms of a perturbative expansion of the crystal Hamiltonian and calculated using diagramatic techniques, in the framework of the Green's-function theory.[3] The lowest-order processes involve squares of the cubic terms of the crystal Hamiltonian and describe the transfer of the energy of the optical phonon to other phonon states. In the Van Hove expansion parameter λ of the Hamiltonian, these depopulation processes are of order λ^2 and give rise, when $kT \geq \hbar\omega$, to a linear variation of the inverse lifetime with T. Higher-order processes of order λ^4 involve squares of quartic terms of the crystal Hamiltonian or products of cubic and quartic terms and give rise to a quadratic dependence of the inverse lifetime with T.

One of the most studied systems for the determination of the mechanisms controlling the finite phonon lifetime is crystalline CO_2.[4–6] In particular, very precise measurements of the bandwidth of the three Raman-active lattice modes E_g at 75 cm^{-1}, T_g^- at 93 cm^{-1} and T_g^+ at 136 cm^{-1}, have been made by high-resolution Raman spectroscopy by Ranson, Ouillon, and Califano.[5] The width of these three Raman-active phonons shows an almost perfect quadratic dependence on the temperature. According to the theory of anharmonic lattice dynamics,[3] phonon-phonon coupling processes of order λ^4 in the perturbative expansion of the crystal self-energy are responsible for this nonlinear temperature variation.

A theoretical calculation of the contributions of λ^4 processes to the bandwidth of the lattice phonons of CO_2 as a function of temperature has been recently performed using the Green's-function technique by Jindal, Righini, and Califano.[7] They have shown that the contribution of the λ^4 processes to the overall relaxation is far from being negligible at temperatures above 50 K and have determined the relative importance of the different processes.

Despite the approximations used in the evaluation of the multiple-phonon density of states, these calculations gave a fairly good fit of the experimental Raman results. Even if experimental data were not available at the time, the calculations were extended to the two infrared-active lattice modes T_u^+ at 117 cm^{-1} and T_u^- at 68 cm^{-1}, and also, for them, a nonlinear evolution of the bandwidth

with temperature was predicted.

Experimental data on infrared bandwidths of molecular crystals are actually extremely scarce.[8] The main reason is that, for absorption measurements in the far infrared, extremely thin crystal slabs, of the order of few tens of micrometers, are required, this being a major experimental problem in the infrared spectroscopy of crystalline materials. A second reason is that lattice phonon bands are often very narrow, especially at very low temperatures, and therefore high-resolution far-ir spectrometers are necessary for precise bandwidth measurements.

The availability in our laboratory of a high-resolution Fourier-transform interferometer for the far-infrared region has prompted us to develop a cell in which thin single crystals can be grown from the liquid at low temperatures. This cell has been successfully used to grow single crystals of suitable thickness for several simple molecular crystals, including N_2, N_2O, CS_2, OCS, etc. In this paper we report on the measurement of the bandwidth of the two infrared-active lattice phonons of CO_2 as a function of temperature by high-resolution Fourier-transform infrared spectroscopy (FTIR). In order to obtain a consistent interpretation of the energy-transfer processes in this crystal, we have also reconsidered the interpretation of the Raman data.

II. EXPERIMENT

Reagent-grade CO_2, of purity better than 99.995%, was used. The ir spectra were recorded with the help of a Bruker IFS 120 HR Michelson interferometer equipped with a He-cooled Si bolometer, a cold filter, a 12-μm Mylar beam splitter, and a mercury lamp as source.

The crystal is cooled in a cell attached to a closed-cycle cryotip mounted on an *xyz* table, which permits insertion in the sample chamber of the interferometer and adjustments in the optical path for maximum transmittance. The cryotip is linked to the interferometer through shock-absorbing bellows. The cell can be used with different window material both in the far- and near-ir region as well as for Raman-scattering measurements.

Single crystals were grown from the liquid under pressure. A schematic drawing of the cell is shown in Fig. 1. A copper block with a hole for insertion of the windows is held in tight contact to the cold finger of the cryotip. Two sapphire windows separated by a spacer of the desired thickness are inserted in the hole. Perfect sealing of the cell is ensured by indium gaskets outside the windows, as shown in the figure. In this way the material between the windows is in direct contact with the copper block, which ensures good thermal contact. The gas inlet consists of a flexible 1-mm steel capillary, which allows the gas from the handling system to reach the small volume between the windows. The capillary is kept warm by a heater to avoid condensation of the gas before it reaches the active volume. The temperature of the cell is monitored by two calibrated Si diodes with an uncertainty of less than ± 1 K. The diodes are held in contact to the copper block, one above and the other below the cell. In this way it is possible to measure and control the temperature gradient in the cell by varying the current in

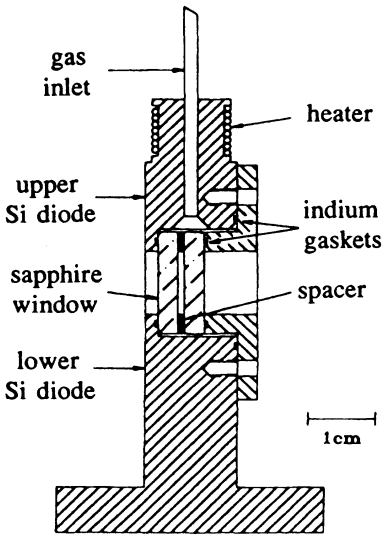

FIG. 1. Schematic drawing of the variable-thickness low-temperature cell single-crystal growth.

the capillary heater. This temperature gradient is important in the growth process. Temperature differences between the two diodes from 2 to 20 K near the melting points were maintained for different materials.

The procedure for crystal growth is as follows. The temperature is lowered to about 220 K at the lower diode; the cell is filled with CO_2 through the capillary at a pressure of 6 bars with a gradient of 10 K between the upper and lower parts of the cell (for comparison the triple point of CO_2 is 216 K at 5 bars). When liquid CO_2 fills completely the cell, it is shock frozen within few minutes to a temperature 5 K lower. The strongly scattering polycrystalline sample obtained in this way is warmed up slowly, until only a small seed remains in the coldest region ($T \approx 216$ K) of the cell. After few fusion and crystallization cycles, a perfect transparent seed can be easily obtained. The cell is then kept at constant temperature under visual control of the dimension and transparency of the seed. The temperature is then lowered at a speed of about 0.1 K per hour, allowing the crystal to grow from the seed. The soft crystal grown in this way, made of few monocrystalline domains, is then annealed at the temperature of 215.6 K for several hours. Through this annealing procedure a single domain grows at the expense of the others and eventually fills completely the central part of cell. Afterward the gas inlet is closed and the temperature gradient is slowly eliminated by turning off the capillary heater. The temperature is then lowered at a speed of 5 K/h to the desired value, and the cryotip is inserted in the interferometer. The single crystals obtained with this procedure have always dimensions much larger than that of the ir beam ($\phi < 2$ mm).

The optical quality of the sample is controlled by visual observation between crossed polarizers. In all our experiments perfectly transparent crystals with sharp rectangular edges were obtained. No crystal damage or cracking is normally observed when decreasing the temperature.

Sometimes, however, the crystal surface turns slightly rough because of the different thermal expansions of the crystal and windows.

Because of the presence of four windows, two of poly-4-methyl-pent-1-ene (TPX) for the cryotip and two of sapphire for the cell, the intensity of the light transmitted through the sample is reduced to about 10% of that of the impinging ir beam. In order to increase the sensitivity of the instrument, measurements were made by pumping on the liquid He in the bolometer.

In the analysis of the data, one has to face the difficulty that, because of the very small thickness of the sample and the presence of the windows, strong interference fringes due to the beating of at least two separate frequencies are superimposed on the spectrum. Both frequencies are directly related to the cell dimensions. In the interferogram the signals due to the faster modulation fall in a region well separated from that carrying information on the spectrum of the sample. By blanking the corresponding spot of the interferogram, these fringes were almost completely eliminated from the spectrum. This has no influence on the band shape, as can be seen from Fig. 2, which shows the T_u^+ band at 117 cm^{-1} before and after correction of the interferogram. The signals due to the slower modulation fall in a region which overlaps that of the bands and therefore cannot be eliminated by the same technique without affecting the band shape. For this reason and since this modulation does not introduce any serious error in the bandwidth measurements, as can be seen from Fig. 2, no further attempt to eliminate this effect was made.

Both bands overlap an absorption continuum whose intensity increases steadily with increasing frequency in the range from about 60 to 130 cm^{-1} covered in our measurements. Since the two-phonon density of states,[9] extending from about 50 to 250 cm^{-1}, increases with frequency up to about 170 cm^{-1}, we assign this absorption to a weak activity due to anharmonic effects of the underlying two-phonon density of states. The intensity of the two ir-active phonons is actually very weak because of the absence of a dipole moment on the molecules, and therefore it is expected to be comparable with that of the two-phonon density of states, since both acquire ir intensity through second-order mechanisms. In addition, surface effects may also contribute to this band asymmetry at higher frequencies. For the definition of the base line, this absorption continuum was subtracted from the spectrum.

When the temperature of the sample is lowered, the bands narrow and the peak intensity increases. In order to keep the peak intensity at a reasonable value, between 1 and 2 absorbance units, we used at different temperatures different sample thicknesses, ranging from 10 to 100 μm. For convenience two different spacers were used in each experiment, a thinner one in the upper-half part and a thicker one in the lower-half part of the cell. We used 10–25 μm spacers below 20 K, 25–50-μm spacers between 20 and 70 K, and a single 100-μm spacer between 70 and 100 K. Care was taken to repeat the measurements with different spacers in the overlapping temperature regions, in order to control the reproducibility of the data.

The instrumental function (a trapezoidal apodization function) used was always at least one order of magnitude smaller (<0.05 cm^{-1}) than the width of the bands, and therefore no band deconvolution was made. By a nonlinear least-squares fitting, based on the Marquardt algorithm, the bands were analyzed for their Lorentzian or Gaussian character. Both bands show, in the complete temperature range examined, a perfect Lorentzian shape, as can be seen from Fig. 3, where the bands are shown in

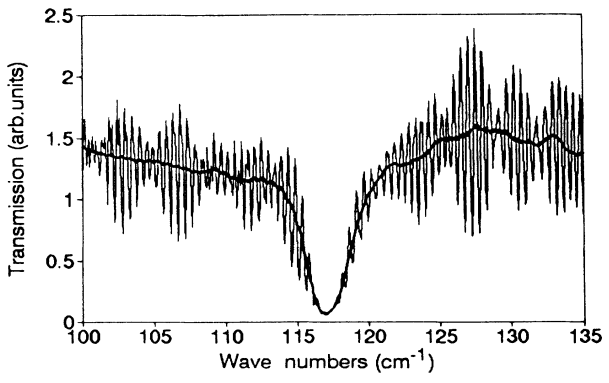

FIG.2. Single-beam spectrum of the T_u^+ absorption band before and after elimination of the interference fringes by correction of the interferogram.

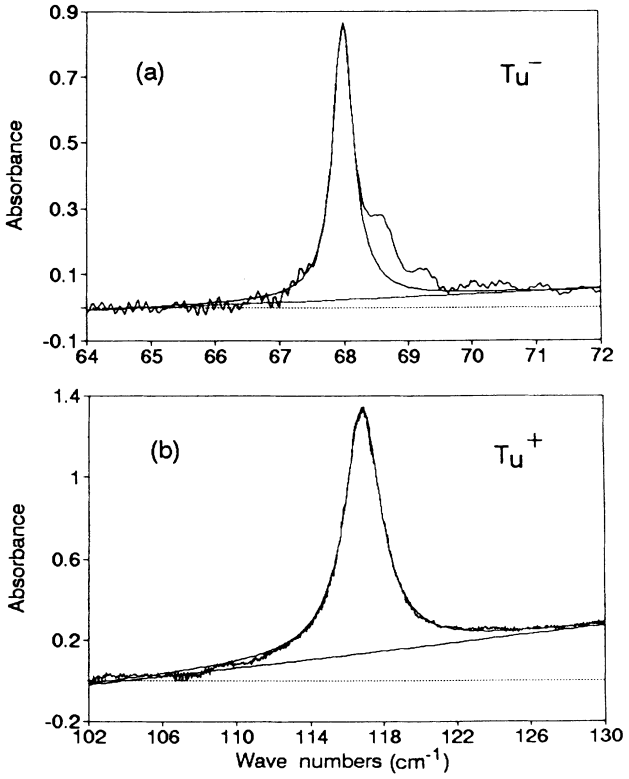

FIG. 3. Absorbance spectra of the two ir-active lattice modes of crystalline CO_2. In each part is also shown the Lorentzian curve that fits the band profile and base line. (a) T_u^- phonon ($T=45$ K) and (b) T_u^+ phonon ($T=30$ K).

absorbance together with the corresponding Lorentzian functions which fit the band profiles.

Bandwidth errors due to the fitting procedure are $\pm 0.01\ cm^{-1}$ at 18 K and $\pm 0.2\ cm^{-1}$ at 90 K. Errors in the absolute frequency of the band peaks due to the inherent calibration of the instrument by a He-Ne laser are of the order of $\pm 0.01\ cm^{-1}$.

III. RESULTS AND DISCUSSION

CO_2 crystallizes in the cubic system space group $Pa3$ (T_h^6) with four molecules per unit cell and possesses seven optical lattice modes, three librations E_g, T_g^-, and T_g^+ active in Raman, two translations T_u^- and T_u^+ active in infrared, and two modes A_u and E_u inactive in both spectra. The frequency and bandwidth of the three Raman-active lattice phonons have been recently measured in a wide temperature range by Ranson, Ouillon, and Califano.[5] We have measured under high resolution the absorption profile of the two ir-active lattice phonons at several temperatures, in the range 12–100 K, to obtain their frequency and bandwidth. Measurements were limited to this temperature interval because the tail of the absorption band of the sapphire windows shifts with increasing temperature toward lower frequency and cuts off the transmission above 100 K. The frequencies of the five optical modes at low temperature and the results of the calculations of Ref. 7 are listed in Table I.

The bandwidths $\Gamma(T)$ of the two infrared-active phonons are plotted as a function of T in Fig. 4. For a general discussion of the relaxation processes contributing to the lifetime of the CO_2 lattice phonons, we show in Fig. 5 the corresponding evolution with temperature of the bandwidths of the three Raman-active phonons.

For an analysis of the relevant relaxation mechanisms controlling the lifetime of these phonons, we shall rely mostly on the results of the calculations of Jindal,

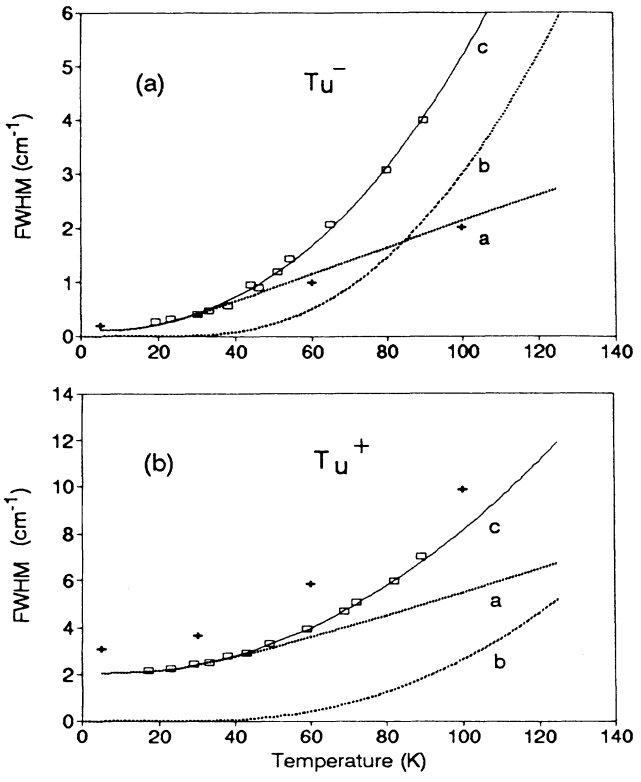

FIG. 4. Bandwidth (full width at half maximum) of the two ir-active lattice phonons of CO_2 as a function of temperature. Open squares, experimental data; crosses, calculated width from Ref. 7; curves *a*, three-phonon processes; curves *b*, quartic processes; curves *c*, sum of curves *a* and *b*. (a) T_u^- phonon and (b) T_u^+ phonon.

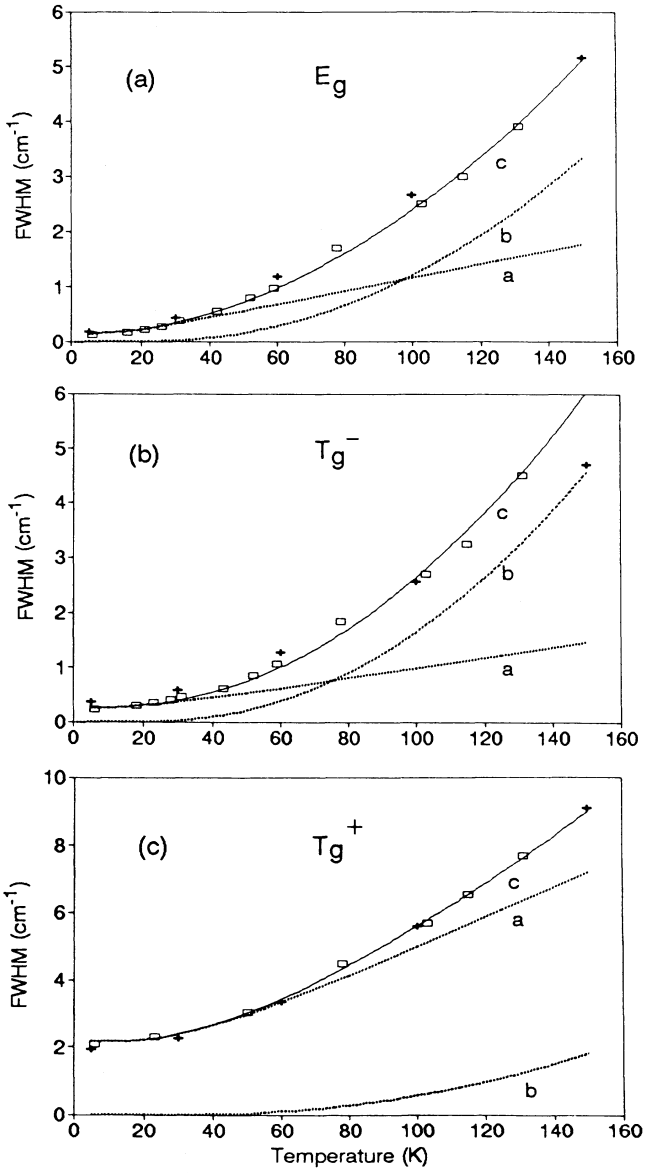

FIG. 5. Variation with temperature of the bandwidth (full width at half maximum) of the three Raman-active lattice phonons of CO_2. Open squares, experimental data; crosses, calculated width from Ref. 7; curves *a*, three-phonon processes; curves *b*, quartic processes; curves *c*, sum of curves *a* and *b*. (a) E_g phonon, (b) T_g^- phonon, and (c) T_g^+ phonon.

TABLE I. Low-temperature frequencies (in cm^{-1}) of the optical lattice phonons of crystalline CO_2.

Mode	ω_{expt} This work	Ref. 5[a]	ω_{calc} Ref. 7
T_u^-	68.1[b]		75.2
E_g	74.8[c]	75.5	74.9
T_g^-	93.3[c]	93.5	87.0
T_u^+	117.0[b]		118.4
T_g^+	134.5[c]	135.9	135.9

[a] $T=6$ K.
[b] $T=25$ K.
[c] $T=18$ K.

Righini, and Califano.[7] These reproduce correctly the nonlinear variation with temperature of the three Raman-active phonons and predict a similar nonlinear behavior for the two infrared-active phonons. In particular, the calculations show that in this case the width $\Gamma(0)$ at $T=0$ of the T_u^- phonon should be more than one order of magnitude smaller than that of the T_u^+ phonon. Both predictions are verified by our measurements, although no quantitative agreement is found between calculated and observed values. In particular, in the case of the T_u^- phonon, the calculations of Ref. 7 agree almost perfectly with experiments at very low temperature, but diverge at temperatures higher than 40 K. In the case instead of the T_u^+ phonon, the calculated values are always higher than the experimental ones, although they show the same type of temperature dependence.

In order to obtain a better agreement between theory and experiments, we discuss first the approximations involved in the calculations of Ref. 7. For an exact calculation up to the λ^4 order, multiple Brillouin-zone summations up to five different wave vectors $\mathbf{k}_i$, as well as sums over all branches j and on several phonon propagators, are required. This is obviously an impossible task even with the largest available computers. For this reason approximate calculations were made, restricting the $\mathbf{k}$ sums to a single special point of the Brillouin zone and summing over all branches. This point was chosen so that the widths calculated at the λ^2 order would not differ appreciably from those calculated using the whole scan of the Brillouin zone.

The most relevant conclusions of these calculations concern the relative importance of the contribution to the width of the different λ^2 and λ^4 diagrams. The largest contribution to the bandwidth arises from the second-order diagrams (a) and (b) of Fig. 6. At the λ^4 order, diagram (c), with two quartic vertices, gives a negligible contribution, whereas the only diagrams that play a significant role are the diagrams (d), (e), (g), and (h), which involve cubic vertices. These results were recently confirmed by a detailed analysis of the relaxation processes in linear chains of diatomic and triatomic molecules[10] for which the contribution of all these diagrams can be exactly calculated. As a further check, we have done, as part of an extensive calculation of the relaxation processes in crystalline CO_2, an exact calculation of the contribution of diagram (c) and we have confirmed that it is negligible.

On the basis of these results, we have used the following approach. According to the theory of anharmonic processes in crystals,[3,11] the contributions of the three-phonon down-decay processes ($3d$) of diagram (a) of Fig. 6 and of the three-phonon up-decay processes ($3u$) of diagram (b) to the bandwidth of an optical phonon, belonging to the j branch with $\mathbf{k}=0$ wave vector can be written as

$$\Gamma_{j0}^{(3d)}(T)=36\pi\hbar^{-2}C^2\sum_k\sum_{a,b}\frac{(1-e^{r\omega_a})^2(1-E^{r\omega_b})^2}{(\omega_{j0}\omega_{ak}\omega_{b-k})}[(n_{ak}+n_{b-k}+1)\delta(\omega_{j0}-\omega_{ak}-\omega_{b-k})] \tag{1}$$

and

$$\Gamma_{j0}^{(3u)}(T)=72\pi\hbar^{-2}C^2\sum_k\sum_{a,b}\frac{(1-e^{r\omega_a})^2(1-e^{r\omega_b})^2}{(\omega_{j0}\omega_{ak}\omega_{b-k})}[(n_{ak}-n_{b-k})\delta(\omega_{j0}+\omega_{ak}-\omega_{b-k})]\ , \tag{2}$$

respectively. Here C is the average of the cubic derivatives of the crystal potential V with respect to the crystal normal coordinates Q_{j0}, Q_{ak}, and Q_{b-k}, coupling the phonons ω_{j0}, ω_{ak}, and ω_{b-k} with total momentum conservation $k=k_a+k_b=0$,

$$C_{j0,ak,b-k}=\left|\frac{\partial^3 V}{\partial Q_{j0}\partial Q_{ak}\partial Q_{b-k}}\right|\ , \tag{3}$$

and the factor $(1-e^{r\omega_a})(1-e^{r\omega_b})$, where $r=1/\omega_c$, takes care of the fact that these coefficients must converge to zero as either ω_a or ω_b goes to zero.[11] The cutoff frequency ω_c is chosen equal to 15 cm^{-1}, for a correct smoothing of the coupling coefficients in the region of the acoustic phonons. The delta functions $\delta(\omega_{j0}\pm\omega_{ak}$

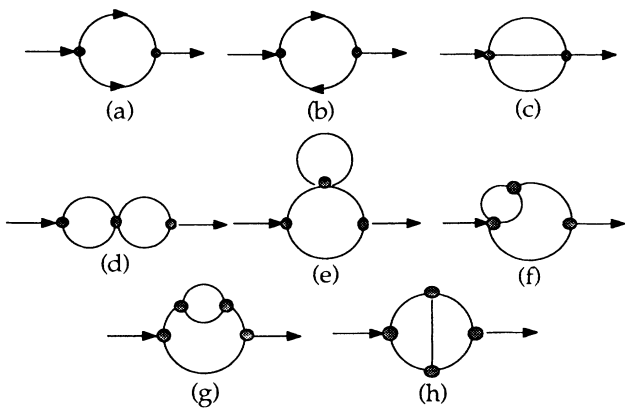

FIG. 6. Diagrams of order λ^2 and λ^4 contributing to the self-energy.

TABLE II. Bandwidth at $T=0$, cubic C, and quartic A coupling coefficient, average bath phonon frequency ω_i, and $(\Delta\omega/\Delta T)_p$ for the optical phonons of crystalline CO_2.

Mode	ω (cm^{-1})	$\Gamma(0)$ (cm^{-1})	C (cm^{-1})	A (cm^{-1})	ω_i (cm^{-1})	$(\Delta\omega/\Delta T)_p$ (cm^{-1}/K)
T_u^-	68.12	0.12	0.0804	1.4	38	0.02
E_g	74.85	0.14	0.0471	0.63	38	0.05
T_g^-	93.29	0.26	0.0246	1.5	47	0.07
T_u^+	117.01	2.06	0.0341	4.8	59	0.07
T_g^+	134.5	2.16	0.0312	1.7	68	0.10

$\pm\omega_{b-k}$) ensure energy conservation in the processes and the n_i are the statistical phonon occupation numbers, given by

$$n_i=(e^{\hbar\omega_i/kT}-1)^{-1}\ . \tag{4}$$

With the aid of Eqs. (1) and (2), we have calculated the contribution of the three-phonon decay processes to the bandwidth of the two ir and three Raman-active phonons in the temperature range considered. At $T=0$ only the down processes of Eq. (1) contribute to the $\Gamma(0)$ width. The C coefficients were thus determined for all five bands by fitting the experimental value of $\Gamma(0)$ by means of Eq. (1). The calculated coefficients are listed in Table II, together with the corresponding $\Gamma(0)$ values. The sum of $\Gamma^{(3d)}$ and $\Gamma^{(3u)}$ is plotted as a function of T in Figs. 4 and 5 (a curves).

We consider now the diagrams of λ^4 order. The contribution of all λ^4 diagrams to the bandwidth can be obtained by evaluating the imaginary part of their self-energy terms, given in all details in Ref. 10. As discussed before, the contribution of diagram (c) of Fig. 6 is proved to be vanishingly small and we shall not consider it any

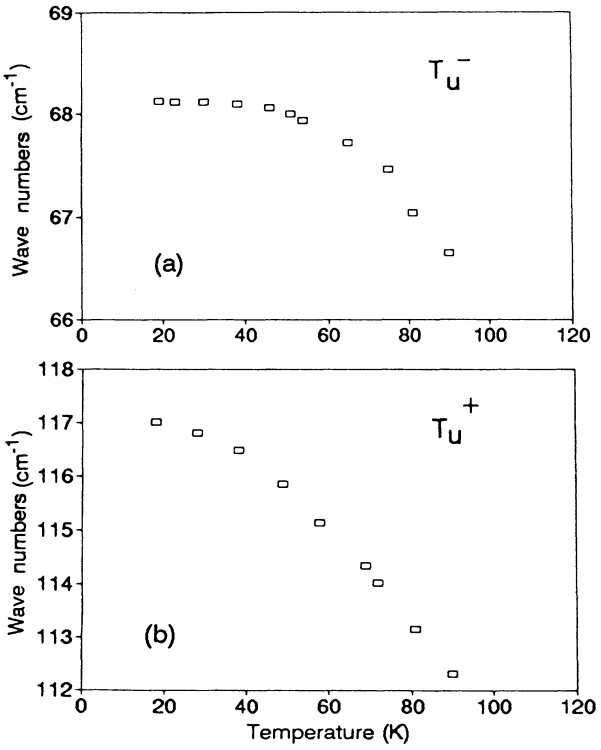

FIG. 7. Variation with temperature of the frequency of the two ir-active lattice phonons of CO_2. (a) T_u^- phonon and (b) T_u^+ phonon.

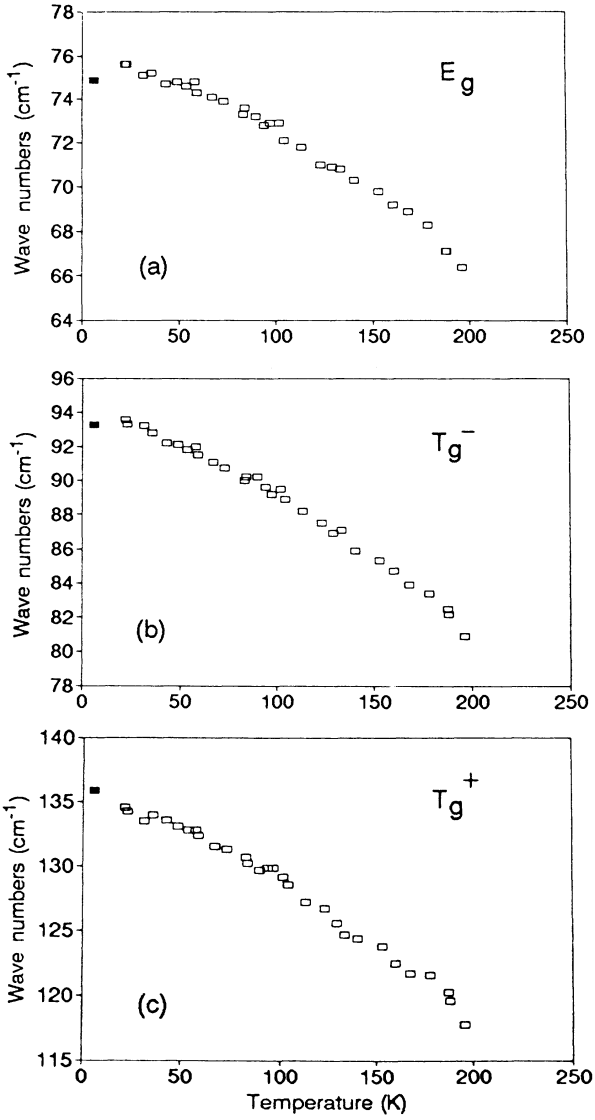

FIG. 8. Variation with temperature of the frequency of the three Raman-active lattice phonons of CO_2. The frequencies were measured with a tandem spectrometer-interferometer at the University of Kaiserslautern (open squares). The solid squares are taken from Ref. 5. (a) E_g phonon, (b) T_g^- phonon, and (c) T_g^+ phonon.

further. Those of diagrams (d), (e), (g), and (h) are all of the same type, that of diagram (g) being by far the most important one. Its contribution to the bandwidth is proportional to the square of a phonon occupation number, to products of four cubic coupling coefficients, and of three different two-phonon density of states. In principle, these diagrams contribute also to $\Gamma(0)$, but as shown in Refs. 7 and 10, this contribution is very small and can be confidently neglected.

As discussed above, a full calculation of these contributions is an enormous task and cannot be faced without severe approximations as those used in Ref. 7. In our laboratory we are developing an algorithm which should allow us to perform the full calculations with reasonable computer time without drastic approximations.[12] This algorithm is based on the results of Ref. 9, which show that the nth-order density of states can be expressed in terms of that at the $n-1$ order and on a redefinition of the phonon creation and annihilation operators. Such calculations are, however, far beyond the scope of the present work. We shall therefore limit ourselves to consider only diagram (g), assuming that its contribution is the dominant one and can represent that of all other diagrams at the λ^4 order. This contribution, according to the discussion above, is written in the simple form

$$\Gamma^{(4)} = A n_i^2 , \tag{5}$$

where A is a parameter and n_i is the occupation numbers of a bath phonon ω_i taken as representative of the average of all phonons involved in the processes. Using for ω_i a frequency of about one-half of that of the phonon considered and adjusting the A parameter, we obtained curves b of Figs. 4 and 5. Curves c in both figures are the sum of the two curves a and b. The fact that curves c fit perfectly the experimental data makes us confident of the validity of the approximation used. The values of ω_i and the A coefficients are listed in Table II.

Further information on anharmonic processes in crystals is supplied by the variation with temperature of the phonon frequency. This type of information is more difficult to analyze in terms of elementary relaxation processes since, as shown in Ref. 10, in contrast to the bandwidths, the anharmonic frequency shifts do not converge at the λ^4 order and require extension of the perturbative expansion to higher orders. For this reason we shall limit ourselves to present in Figs. 7 and 8 the experimental data on the temperature dependence of the five optical-phonon frequencies, without any discussion of the mechanisms involved.

From the slope of the curves of the phonon frequencies versus temperature, we have determined the corresponding $(\Delta\omega/\Delta T)_p$ listed in the last column of Table II. The $(\Delta\omega/\Delta T)_p$ increase systematically with the phonon frequency from 0.02 to 0.10 cm^{-1}/K, following the corresponding increase in the phonon density of states, i.e., the number of processes responsible for the overall relaxation.

ACKNOWLEDGMENTS

This work was supported by the Italian Ministry of University and Scientific and Technological Research and by the C.N.R. We thank Dr. P. Procacci for his aid in the calculations and for helpful discussions. One of us (H.J.J.) wishes to thank the Deutsche Forschungsgemeinschaft for support under Grant No. Jo 86-8.

*Present address: Chemistry Department, University of Florence, Via Gino Capponi 9, 50121 Florence, Italy.

†Present address: Fachbereich Physik, Universität Kaiserslautern, Erwin Schrödinger Strasse, 6750 Kaiserslautern, Germany.

[1] P. Ranson, R. Ouillon, and S. Califano, J. Raman Spectrosc. **17**, 155 (1986), and references therein.

[2] I. S. Velsko and R. M. Hochstrasser, J. Phys. Chem. **89**, 2240 (1985); D. D. Dlott, Annu. Rev. Phys. Chem. **37**, 157 (1986); S. Califano, in *Applied Laser Spectroscopy,* Vol. 241 of *NATO Advanced Study Institute, Series B: Physics,* edited by W. Demtröder and M. Inguscio (Plenum, New York, 1990).

[3] S. Califano, V. Schettino, and N. Neto, *Lattice Dynamics of Molecular Crystals,* Springer Series on Lecture Notes in Chemistry, Vol. 26 (Springer, Berlin, 1981); S. Califano and V. Schettino, Int. Rev. Phys. Chem. **7**, 19 (1988).

[4] J. W. Schmidt and W. B. Daniels, J. Chem. Phys. **73**, 4848 (1980).

[5] P. Ranson, R. Ouillon, and S. Califano, J. Chem. Phys. **89**, 3592 (1988).

[6] G. M. Gale, P. Schanne, and P. Ranson, Chem. Phys. **131**, 455 (1989).

[7] V. K. Jindal, R. Righini, and S. Califano, Phys. Rev. B **38**, 4259 (1988).

[8] R. Bini, P. Foggi, P. Salvi, and V. Schettino, J. Phys. Chem. **94**, 6653 (1990).

[9] R. Della Valle and G. Cardini, Phys. Rev. Lett. **59**, 2196 (1987).

[10] P. Procacci, G. Cardini, R. Righini, and S. Califano, Phys. Rev. B (to be published).

[11] I. P. Ipatova, A. A. Maradoudin, and R. F. Wallis, Phys. Rev. **155**, 882 (1967).

[12] P. Procacci and R. G. Della Valle (unpublished).

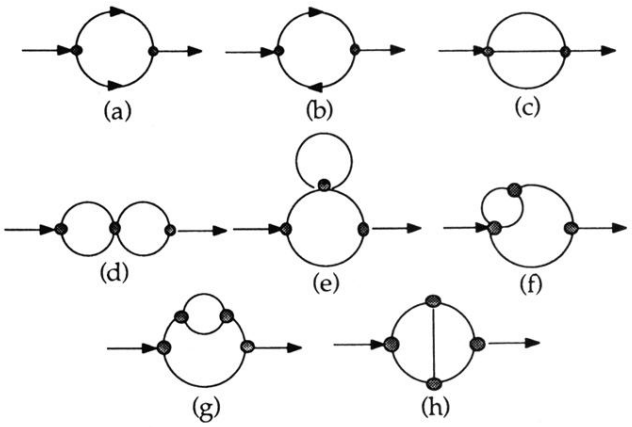

FIG. 6. Diagrams of order λ^2 and λ^4 contributing to the self-energy.